

# Autonomus UAV Cansat for Meteorological Studies

## Team 110 Project Technical Report for the 2021 Latin American Space Challenge

Luis F. Niño<sup>1</sup>, Carlos D. Arenas<sup>2</sup>, Oscar I. Ayala<sup>3</sup> and Julián Rodríguez-Ferreira<sup>4</sup>

*Universidad Industrial de Santander, Bucaramanga, Colombia, 680002*

This document presents a technical advance of an unmanned aerial vehicle CanSat prototype within the framework of the GuaneSat mission developed by the SCUA rocketry team (Semillero de Cohetería UIS Aeroespacial) that will be ejected at a height of approximately 1 km, using as launch vehicle the Falcon UIS, a high power rocket developed by the same group as part of the LASC (Latin American Space Challenge) 2021. The CanSat is designed to collect information on atmospheric variables such as barometric pressure, temperature, levels of particles per million of volatile organic compounds, humidity, carbon dioxide, carbon monoxide, nitrogen dioxide and ammonia , in order to develop vertical atmospheric profiles essential for the study of climate. It will have inertial sensors, which together with a GPS and a magnetometer will allow a safe and controlled descent near the launch site, thus facilitating its recovery. The information of the different variables will be sent wirelessly to a ground station by means of LoRa radio modules. The CanSat glider will have a pair of folding wings and a tail thrust vectoring control mechanism that will occupy a cylindrical volume of 66mm in diameter and 110mm in height, a pair of actuators and a thruster to improve the controllability of the system and thus allow a controlled spiral descent.

### Nomenclature

<i>LDO</i>	= Low Dropout Regulator
<i>GPS</i>	= Global Positioning System
<i>IMU</i>	= Inertial Measurement Unit
<i>tVOC</i>	= Total Volatile Organic Compounds
<i>CO<sub>2</sub></i>	= Carbon Dioxide
<i>CO</i>	= Carbon Monoxide
<i>NO<sub>2</sub></i>	= Nitrogen Dioxide
<i>NH<sub>3</sub></i>	= Ammonia
<i>TVC</i>	= Thrust Vectoring Control
<i>EDF</i>	= Electric Ducted Fan
<i>CM</i>	= Center of Mass
<i>UAV</i>	= Unmanned Aerial Vehicle
<i>RTSP</i>	= Real Time Streaming Protocol
<i>PID</i>	= Proportional, Integral and Derivative

### I. Introduction

The monitoring and control of atmospheric pollution is becoming increasingly important, especially in large cities, since according to figures from the World Health Organization, one out of every eight deaths in the world is caused by atmospheric pollution. The daily activity of cities generates a large amount of substances that modify the natural composition of the air we breathe. Vehicles are the main source of air pollutant emissions, followed by industry,

<sup>1</sup>Electronic Engineering , Escuela de Ingeniería Eléctrica, Electrónica y de Telecomunicaciones, luis.nino@correo.uis.edu.co.

<sup>2</sup>Undergraduate, Escuela de Ingeniería Mecánica, carlos.arenas4@correo.uis.edu.co

<sup>3</sup>Undergraduate, Escuela de Ingeniería Mecánica, oscar2172249@correo.uis.edu.co

<sup>4</sup>Professor, Escuela de Ingeniería Eléctrica, Electrónica y de Telecomunicaciones, jgrodrif@uis.edu.co.



households and emissions from natural sources, which produce thousands of tons of pollutants that remain in the atmosphere.

One of the ways to protect people's health is through continuous monitoring and reporting of air quality to take timely action, therefore, we present some advances in the design of an unmanned aerial vehicle CanSat, this is a simulation of a picosatellite with a cylindrical or can shape, it has a weight between 200 to 1000[g], it is usually launched by a rocket that ejects it to a height between 100 to 3000[m] [1, 2]. The CanSat is designed to collect atmospheric variables such as barometric pressure, temperature, humidity and some air quality variables such as particulate matter per million, tVOC, CO<sub>2</sub>, CO, NO<sub>2</sub> and NH<sub>3</sub> levels. With the scientific data generated, we are interested in the analysis of air quality by means of vertical atmospheric profiles. The device will be controlled using inertial sensors, which in conjunction with the GPS and magnetometer will allow a safe and controlled flight [3, 4], landing in the nearby target area, thus facilitating its recovery and reuse. A LoRa RF module will perform communications with its respective ground station. Considering the reusability of the device, the recovery system becomes very important, the CanSat has two folding wings, that gives it the ability to be compact but have a controlled flying while descending [5, 6], and a pair of thrust vectoring turbines in the tail to fly like a glider [7]. Manipulating the angle of each thruster and its thrust force controls the flight dynamics which in turn will control the fall, allowing under a proper control system to follow a downward spiral trajectory [8, 9]. During its ascent, it will be impossible to take data, but once the launch vehicle releases the CanSat, the wings are opened, followed by the activation of the acquisition modules, which will send the data of the atmospheric variables.

The paper begins by addressing the general architecture of the prototype, starting with the different blocks that make up the electronics of the CanSat and describing the different subsystems such as the power subsystem, the payload, the sensors, the flight computer, the control systems, among others. Subsequently, the mechanical components of the system and its structure are discussed, to which a self-locking system was added to keep the wing deployed, as well as a pair of differential vector EDFs to improve performance during descent. Finally, the description of the mission as such, the guidelines and the chronological order of the most important moments during the mission are discussed.

#### A. Mission Patch



**Fig. 1** Mission Patch GuaneSat 2022 [10]

## II. System Architecture Overview

The main objective of the mission is to study the weather through the construction of atmospheric profiles of atmospheric variables, for this purpose a two-unit CanSat (66[mm] diameter and 230[mm] long) is built. The CanSat has a pair of folding wings and a pair of vector turbines that generate thrust in the tail which together with the avionics allow a controlled spiral flight landing near the launch site.

The avionics consists of a flight computer based on ESP32 that communicates via I2C, SPI, UART and GPIOs to different actuators such as turbines and servomotors, and different sensors such as camera, GPS, IMU, temperature, humidity, atmospheric pressure, levels of particles per million, tVOC, CO<sub>2</sub>, CO, NO<sub>2</sub>, NH<sub>3</sub>, among others as shown in the image 2. The flight computer communicates to the ground station through LoRa which gives it a communication link of over 10 [Km], this allows sending flight data and sensor readings to have a record of these and to be able to take remote actions in the case of an emergency.

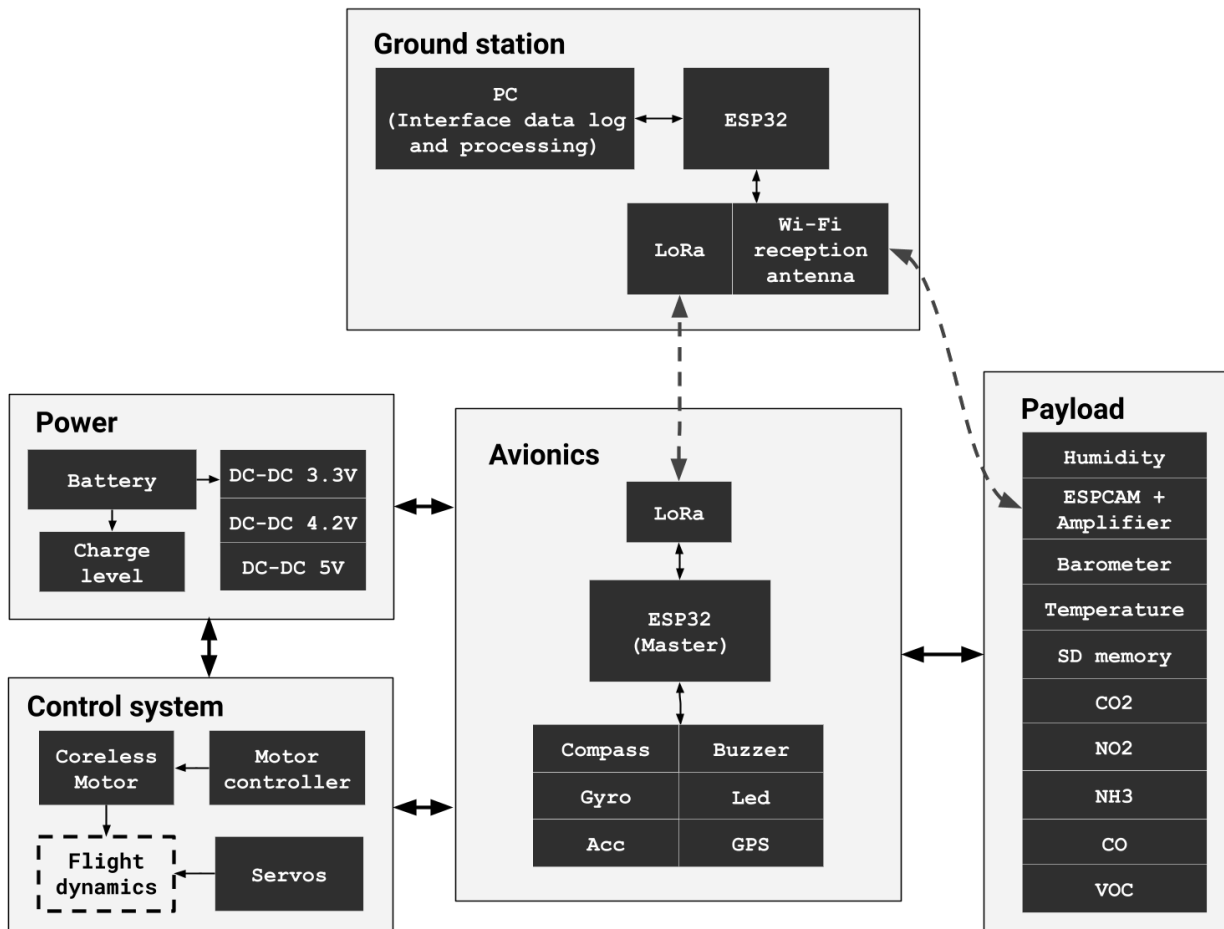


**Fig. 2** CanSat systems description.

### A. Flight computer subsystem:

This is the main subsystem based on an ESP32, where its main functionality is to manage and control the other subsystems. It is connected to an IMU, magnetometer, barometer and GPS to locate it spatially and estimate the actuators control action. The ESP32 will be constantly monitoring the different system parameters to send them to the ground station such as battery level, location, control system variables, payload data among others. For debugging the different phases of the flight there are LED indicators and a buzzer. The table 1 and 2 summarizes the sensors features.

**Table 1 GPS module features**

<b>Reference</b>	<b>Horizontal position accuracy</b>	<b>Maximum update rate</b>
NEO-6M	2.5 m	5 Hz

**Table 2 Sensors features**

<b>Sensor</b>	<b>Measured variable</b>	<b>Range</b>	<b>Sensibility</b>
Accelerometer MPU6050	Acceleration	$\pm 2g / \pm 4g / \pm 8g / \pm 16g$	2 %
Gyroscope MPU6050	Angular speed	$250 ^\circ/s / 500 ^\circ/s / 1000 ^\circ/s / 2000 ^\circ/s$	-
Magnetometer HMC5983	Magnetic field strength	$\pm$ Gauss	LSB/Gauss
BMP180	Atmospheric pressure	300 - 1050 hPa	$\pm 0.12$ [hPa]

**B. Payload subsystem:**

This subsystem is equipped with a OV2640 camera based on an ESP32 and sensors to measure atmospheric variables such as temperature, humidity, atmospheric pressure, levels of particles per million, volatile organic compounds, carbon dioxide, carbon monoxide, nitrogen dioxide and ammonia to determine air quality. These data is recorded in a SD memory as they are transmitted. The tables 3 and 4 summarizes the sensors features.

**Table 3 Sensors features**

<b>Sensor</b>	<b>Measured variable</b>	<b>Range</b>	<b>Sensibility</b>
SHT31	Relative Humidity	0 - 100 RH%	$\pm 2$
SHT31	Temperature	0 - 90[°C]	0.3
BMP180	Atmospheric pressure	300 - 1050 hPa	$\pm 0.12$ [hPa]
CCS811	tCOV	0 - 1187 [ppb]	-
MH-Z14A	CO <sub>2</sub>	0 - 5000 [ ppm]	1[ppm]
MiCS-6814	CO, NO <sub>2</sub> , NH <sub>3</sub>	0 - 1000 [ppm], 0.05 - 10 [ppm], 1 - 500 [ppm]	1.2 [ppm], 2 [ppm] , 1.5 [ppm]
PMS7003	Dust and particulate matter	0 - 1000[ $\mu g/m^3$ ]	1[ $\mu g/m^3$ ]

**Table 4 Camera features**

<b>Sensor</b>	<b>Measured variable</b>	<b>Sensibility</b>
OV2640	Image 2MP 15fps	0.6V/Lux-sec

**C. Communications subsystem:**

In charge of codifying and sending measurements and housekeeping data to the ground station. Communication is established through two LoRa module (this communication has a range of up to 10km). The ground station is composed by a LoRa module and a ESP32 who sends through USB the data to the PC dashboard. In this dashboard the data



is displayed and the graphical results are constructed as the data is received. The camera sends video through RTSP streaming using the ESP32 WiFi and a SBB5089Z 20[dB] amplifier to achieve a 3[km] communication link (to be tested).

#### D. Power subsystem:

To dimension the power subsystem is necessary calculate the consumption of the principal system components , this is presented in the table 5.

**Table 5 Maximum system current consumption**

Component	Current[mA]	Quantity	Subtotal[mA]
ESP32-WROOM-32E	150	2	300
Camera OV2640	0.125	1	0.125
Socket SD Memory	40	1	40
PSRAM64H	0.2	1	0.2
NEO-6M	45	1	45
Lora Ra-02	120	1	120
MPU6050	3.9	1	3.9
BMP180	0.03	1	0.03
SHT31	0.048	1	0.048
CCS811	54	1	54
HMC5983	0.1	1	0.1
MiCS-6814	30	1	30
MH-Z14A	60	1	60
PMS7003	100	1	100
SBB5089Z	100	1	100
Coreless motor	150	2	300
Servo HK-15318S	100	2	200
<b>Average total current consumption [A]</b>			<b>1.32</b>

The subsystem is powered by a Lipo battery of 1000[mAh] at 7.4[V] that powers three DC-DC Buck converters based on a MP2307 capable of providing up to 3[A]. The converters are configured to 3.3[V] to power the microcontrollers, LoRa modules and some sensors, to 4[V] to power coreless motors and servomotors, and to 5[V] to power some other sensors. The OV2640 camera needs 1.2[V] and 2.8[V] to operate, thus two XC6206 LDO are added to the design.

**Table 6 Power subsystem components details**

Component	Description
MP2307	Rectified Step-Down Converter 3A 4.75-23(input) [V]
XC6206 1.2[V]	LDO Voltage regulator
XC6206 2.8[V]	LDO Voltage regulator
Turnigy 10002S20C	1000[mAh] Lipo Battery to 7.4[V]

Considering that once stabilized the servomotors only need a considerable current when they move to make corrections to follow the path due to disturbances, the flight computers ESP32 don't use WiFi, and the coreless motors don't operate at maximum power, we can estimate the total system consumption on 963[mA] and thus estimate the minimum flight time of 60[min].



### E. Control subsystem:

The descent of the CanSat is a challenge that requires a fairly robust control system due to the constant disturbances to which the device will be subjected. The inertial measurements recorded by the sensors must be processed and filtered to obtain the real position during the fall. This information is compared with the position on which the landing is desired to make the respective corrections through the actuators.

The actuators will be two tilttable EDF that form a differential system, allowing to control Roll, Pitch and Jaw, and thus the direction of the CanSat during descent. The device in charge of collecting the inertial measurements will be the MPU6050, the BMP18 will take the height and the HMC5983 the orientation, these data will be processed with the GPS information by a Kalman filter to estimate the spatial position of the CanSat and make the necessary corrections to follow the desired spiral trajectory trough a PID controller.

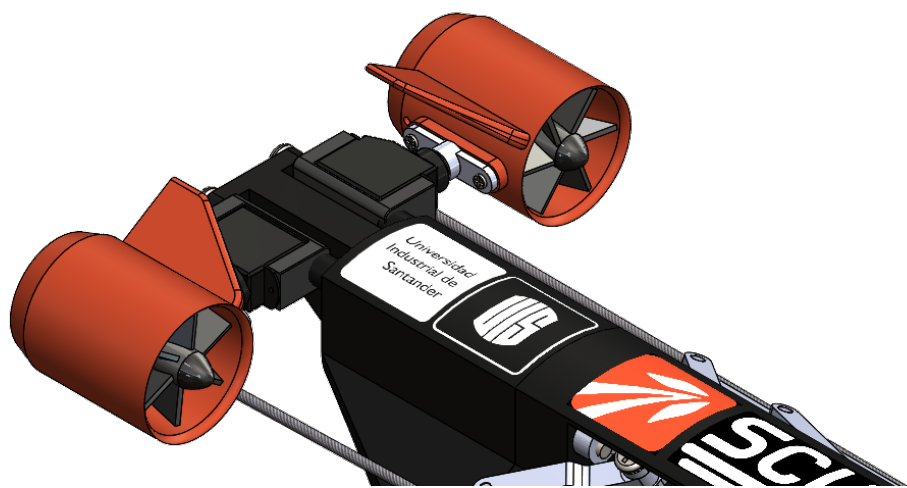


**Fig. 3 System actuators.**

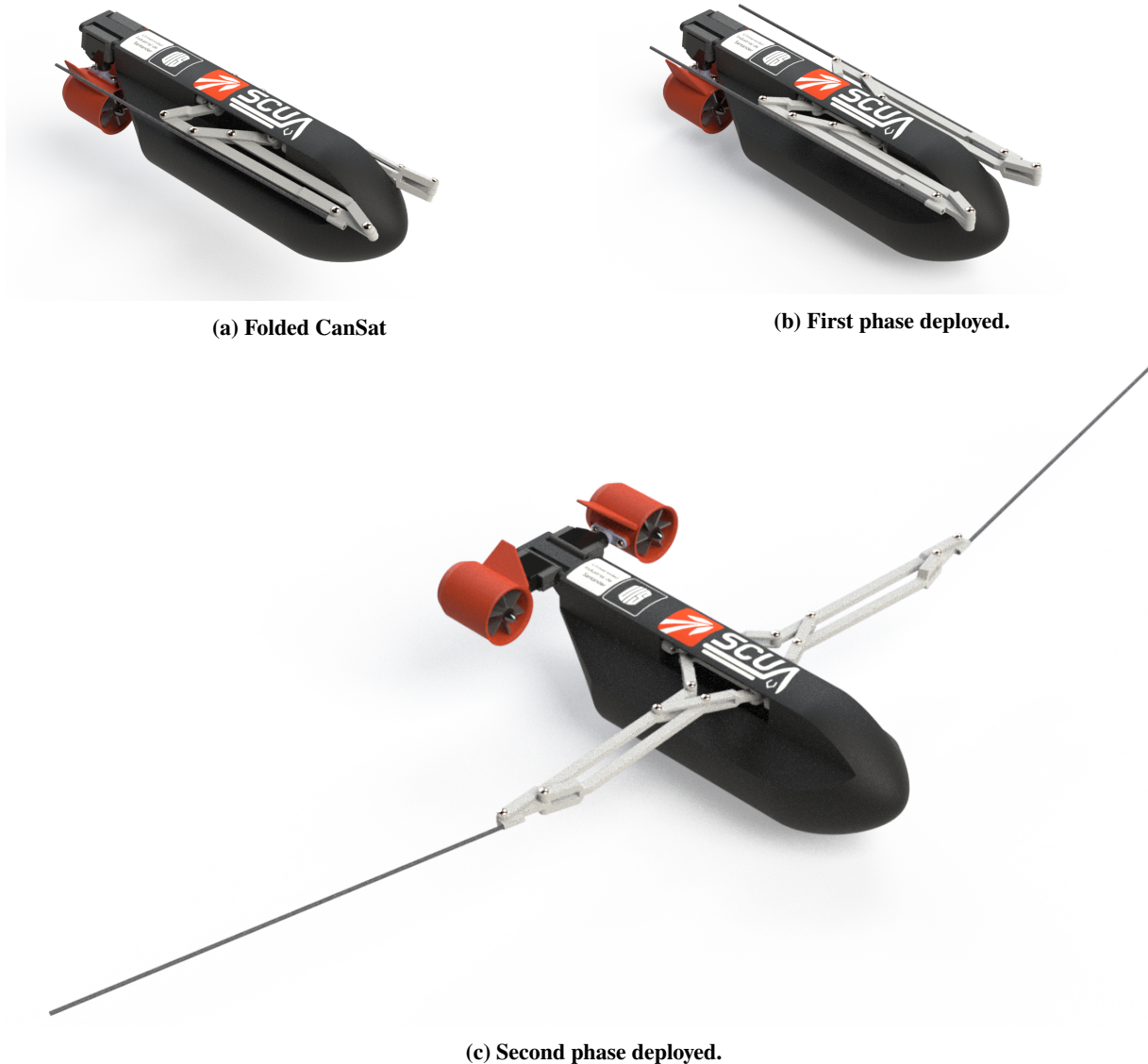
### F. Mechanical Design

The CanSat concept design consists of an aircraft that features bio-inspired foldable wings and a thrust vectoring control (TVC) system consisting of two tilttable electric ducted fans (EDFs) that works as a booster and steering device. The TVC mechanism is deployed as two spring loaded arms positioned at the tail section of the aircraft are released. Each wing structure is based on the movement of bird's wings, this is achieved by two spring actuated four-bar linkage mechanisms and extends a flexible membrane which creates the wing airfoil in order to generate lift. Initially, The aircraft is considered in terms of flying dynamics as a glider as it doesn't need thrust in order to generate lift in the takeoff as it is already launched at a high altitude, however, the thrusters are used to extend the range of the UAV and have the enhanced maneuverability of a vectored thrust vehicle (faster response than conventional surface controls in a considerably more compact volume) [11].

All the electronic components are located within the CanSat structure in two PCBs, these PCBs are connected between them by a FPC band. The motor, servomotors, camera and battery are attached to the structure and all components are located in a compact structure with the size of a two units CanSat, optimizing the space and leaving freedom to improve the air-frame and modify the CM.

The CanSat design is presented in the figure 4, this is a concept design, is necessary to improve the air frame and mass distribution to obtain a stable flight.



**Fig. 4 CanSat mechanical design.**

The idea of using foldable wings was inspired by the biomechanics of birds skeletons, that allow them to have a compact shape when their wings are folded against their body, and have enough lifting area and wingspan when fully deployed to achieve stable flight [5, 12, 13]. This design allowed us to have a convenient way to fit a proper glider in the volume of a CanSat and have enough space to place the internal components. The mechanism consists of two four-bar linkages that are connected in a way that the output angle resulting on the actuation of the first mechanism ( $\theta_2$ ) is used as the input angle for the second one as shown in image 5, where blue bars are the first four-bar linkage mechanism, red bars are the second four-bar linkage mechanism and orange is the line of action of the force applied by the spring.

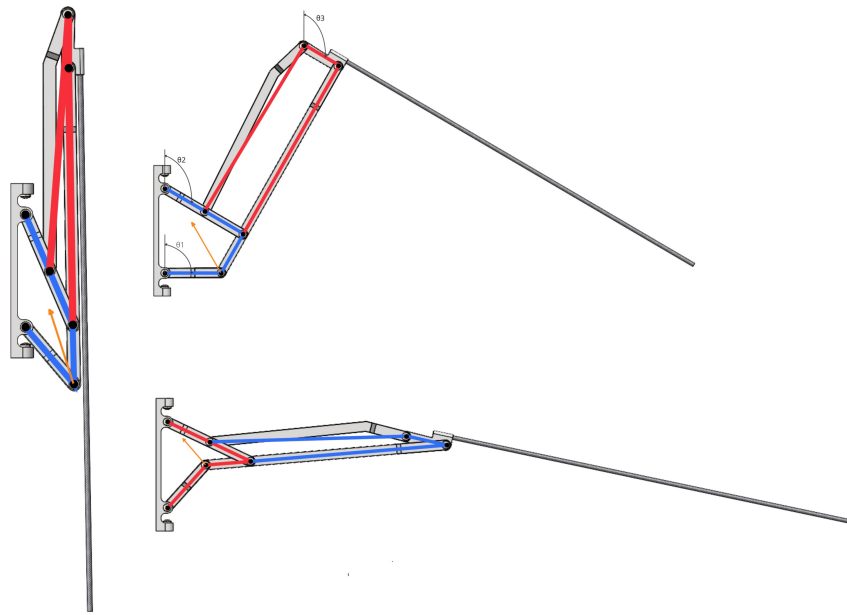


**Fig. 5 wing mechanism.**

In this way, the actuation of the mechanism is reduced to a single linear actuator, more specifically a pre-loaded spring that modifies the angle of the crank link in the first mechanism resulting on a changing in the angle of the rocker link of the linkage that imitates the humerus bone of a bird's wing, and when fully deployed holds the mechanism in a self-locking point that prevents the wing to be folded back. This differs from the way the birds actuate their wings, as they use multiple muscles and tendons to control different sections of the wing while using just one four-bar linkage as seen in image 6.

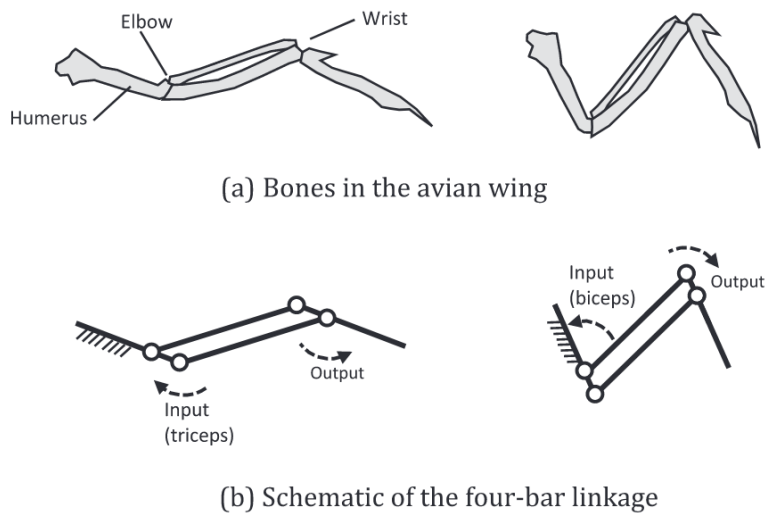


**Fig. 6 Muscle action in a four-bar linkage wing [12]**

The TVC system consists of a coreless DC motor coupled to a propeller, and fitted inside a tube which directs the flow and avoids the vortex generation at the blade tips. Each of the two ducts are tilted by a small servomotor, which modifies the tilt angle with respect to the horizontal plane changing the thrust vector orientation. This mechanism will give us control over the pitch of the aircraft as the two fans move together, as shown in image 7, and over the roll as they are oriented in opposite directions as described in image 8.

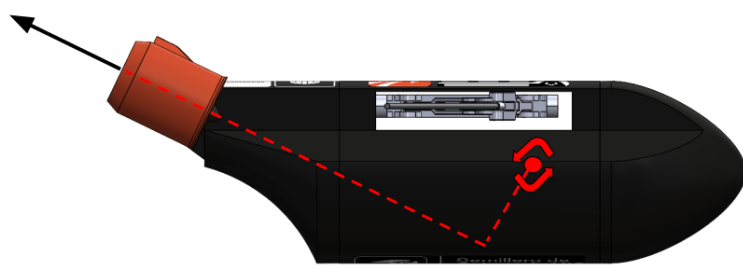


Fig. 7 Pitch movement.

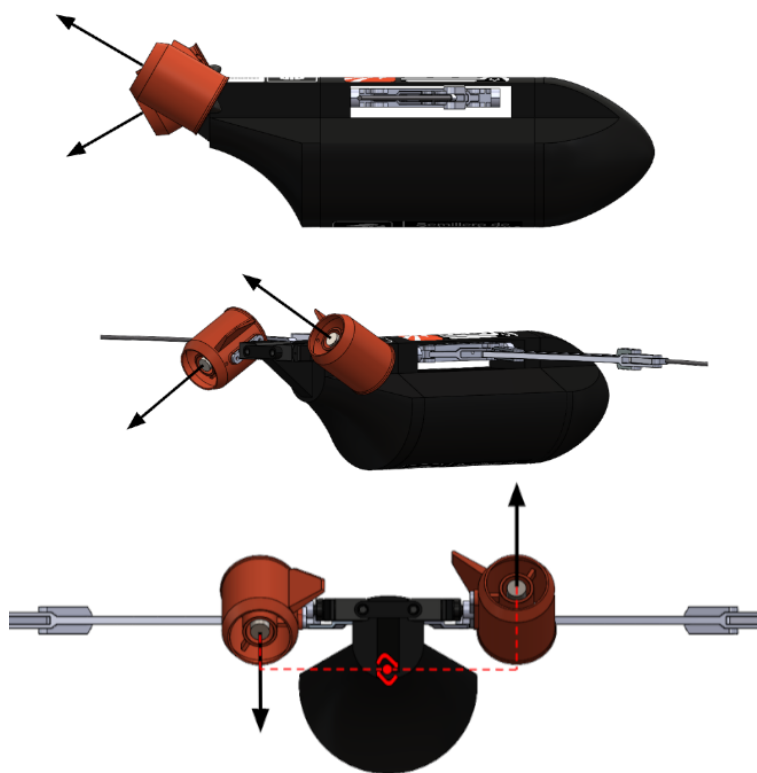
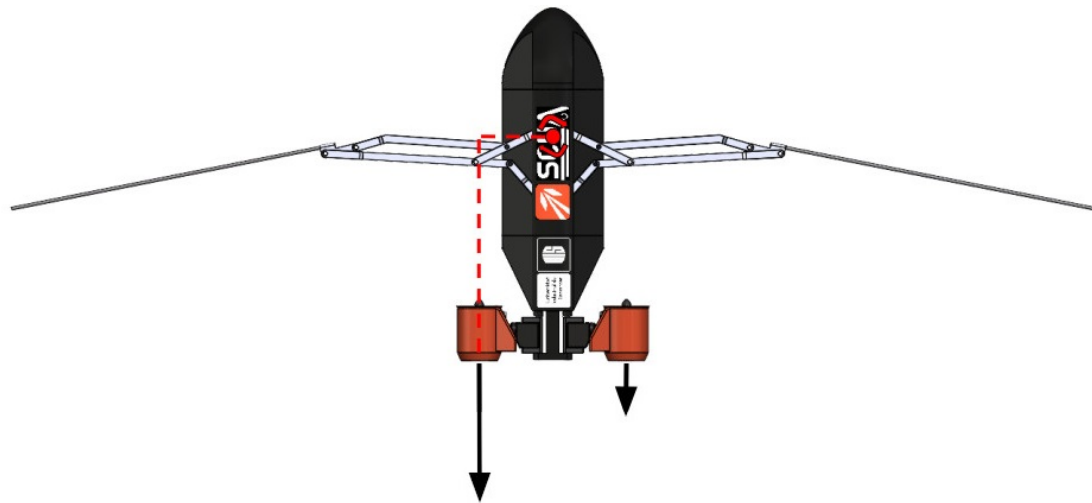


Fig. 8 Roll movement from various vision angles.

The jaw motion will be controlled by differential thrust, decreasing the velocity of one motor and increasing velocity in the other, will cause a torque about the CM, as shown in image 9, where the black arrows show the vector thrust and the red ones show the reaction torque.



**Fig. 9** Jaw movement due to differential thrust.

## References

- [1] Soyer, S., “Small space can: CanSat,” *Proceedings of 5th International Conference on Recent Advances in Space Technologies - RAST2011*, 2011, pp. 789–793. <https://doi.org/10.1109/RAST.2011.5966950>.
- [2] Ramadhan, R. P., Ramadhan, A. R., Putri, S. A., Latukolan, M. I. C., Edwar, and Kusmadi, “Prototype of CanSat with Auto-gyro Payload for Small Satellite Education,” *2019 IEEE 13th International Conference on Telecommunication Systems, Services, and Applications (TSSA)*, 2019, pp. 243–248. <https://doi.org/10.1109/TSSA48701.2019.8985514>.
- [3] Di Luca, M., Mintchev, S., Heitz, G., Noca, F., and Floreano, D., “Bioinspired morphing wings for extended flight envelope and roll control of small drones,” *Interface Focus*, Vol. 7, 2017. <https://doi.org/10.1098/rsfs.2016.0092>.
- [4] Kwak, J., and Sung, Y., “Autonomous UAV Flight Control for GPS-Based Navigation,” *IEEE Access*, Vol. 6, 2018, pp. 37947–37955. <https://doi.org/10.1109/ACCESS.2018.2854712>.
- [5] Jitsukawa, T., Adachi, H., Abe, T., Yamakawa, H., and Umezu, S., “Bio-inspired wing-folding mechanism of micro air vehicle (MAV),” *Artificial Life and Robotics*, Vol. 22, No. 2, 2017, pp. 203–208. <https://doi.org/10.1007/s10015-016-0339-9>, URL <https://doi.org/10.1007/s10015-016-0339-9>.
- [6] Ajanic, E., Feroskhan, M., Mintchev, S., Noca, F., and Floreano, D., “Bioinspired wing and tail morphing extends drone flight capabilities,” *Science Robotics*, Vol. 5, No. 47, 2020, p. eabc2897. <https://doi.org/10.1126/scirobotics.abc2897>, URL <https://www.science.org/doi/abs/10.1126/scirobotics.abc2897>.
- [7] Tanaka, M., Tanaka, K., and Wang, H. O., “Practical Model Construction and Stable Control of an Unmanned Aerial Vehicle With a Parafoil-Type Wing,” *IEEE Transactions on Systems, Man, and Cybernetics: Systems*, Vol. 49, No. 6, 2019, pp. 1291–1297. <https://doi.org/10.1109/TSMC.2017.2707393>.
- [8] Kizilkaya, M. , Oğuz, A. E., and Soyer, S., “CanSat descent control system design and implementation,” *2017 8th International Conference on Recent Advances in Space Technologies (RAST)*, 2017, pp. 241–245. <https://doi.org/10.1109/RAST.2017.8002947>.
- [9] çelebi, M., Ay, S., Ibrahim, M. K., Aydemir, M. E., Bensaada, M., Fernando, L. H. J. D. K., Akiyama, H., and Yamaura, S., “Design and navigation control of an advanced level CANSAT,” *Proceedings of 5th International Conference on Recent Advances in Space Technologies - RAST2011*, 2011, pp. 752–757. <https://doi.org/10.1109/RAST.2011.5966942>.
- [10] Meiga, A., “Eagle bird logo,” , 2022. URL <https://www.vecteezy.com/vector-art/3456052-eagle-bird-logo>, vecteezy.
- [11] Jimenez, A., and Icaza, D., “Thrust Vectoring System Control Concept,” *IFAC Proceedings Volumes*, Vol. 33, 2000, pp. 235–244. [https://doi.org/10.1016/S1474-6670\(17\)35476-9](https://doi.org/10.1016/S1474-6670(17)35476-9).
- [12] Burgess, S., “A review of linkage mechanisms in animal joints and related bioinspired designs,” *Bioinspiration & Biomimetics*, Vol. 16, No. 4, 2021, p. 041001. <https://doi.org/10.1088/1748-3190/abf744>, URL <https://doi.org/10.1088/1748-3190/abf744>.
- [13] Pennycuick, C., *Modelling the Flying Bird*, Academic Press, Academic Press/Elsevier, 2008. URL <https://books.google.com.co/books?id=hHsYIQEACAAJ>.

